Article

Surface Functionalization of Activated Carbon: Coupling of 3-(Aminopropyl)trimethoxysilane and (3-Glycidyloxypropyl)trimethoxysilane

Lucija Pustahija *, Christine Bandl , Sayed Ali Ahmad Alem and Wolfgang Kern †

Institute of Chemistry of Polymeric Materials, Montanuniversität Leoben, 8700 Leoben, Austria;
christine.bandl@unileoben.ac.at (C.B.); ahmad.alem@unileoben.ac.at (S.A.A.A.)
* Correspondence: lucija.pustahija@unileoben.ac.at (L.P)
† Wolfgang Kern passed away.

Abstract: This study aimed to functionalize the surface of activated carbon, and thus render the surface more hydrophilic and reactive. To attain this goal, sequential surface functionalization was carried out using (i) oxidation (pre-activation) and (ii) secondary functionalization. The carbon surface was pre-activated in an autoclave via solvothermal oxidation (i.e., wet oxidation) with nitric acid. Alternatively, plasma-assisted oxidation with a mixture of argon and oxygen (i.e., dry oxidation) was employed. A subsequent step included the reduction in formed carbonyl groups with $LiAlH_4$. Following that, secondary functionalization was performed with 3-(aminopropyl)trimethoxysilane (APTMS) or (3-glycidyloxypropyl)trimethoxysilane (GPTMS), respectively. Changes in the surface composition of carbon after functionalization and morphology were examined by X-ray photoelectron spectroscopy, ATR-FTIR spectroscopy, and scanning electron microscopy. Oxidized carbon samples were successfully modified at their surfaces with APMTS and GPTMS, yielding Si content of 3.2 at. % and 1.9 at. % for wet-oxidized carbon and 5.1 at. % and 2.8 at. % for dry-oxidized carbon, respectively.

Keywords: activated carbon; surface functionalization; solvothermal oxidation; plasma-assisted oxidation; reduction with $LiAlH_4$; APTMS; GPTMS

1. Introduction

Activated carbon is a type of highly porous carbon material. It is initially created by thermally processing carbon-rich biomass like wood, coal, or coconut shells. To enhance the porous surface area of the carbon, various chemical and physical treatments (also known as activation methods) are applied. Activated carbon is primarily used as an adsorbent due to its high specific surface area, making it effective for purifying wastewater and air, as well as in industrial and medical applications in addition to energy storage and catalysis. However, most carbon materials, and this can also be applied to activated carbon, suffer from hydrophobic behavior and a high tendency to form agglomerates. This is especially relevant for the manufacturing of composites, e.g., with matrix polymers such as epoxy resins and polyurethanes. Surface modification techniques are often employed to overcome problems related to dispersibility and enhancing carbon's adsorption properties [1–8]. These techniques mostly rely on attaching different molecules to the carbon surface, such as amines, (organo)silanes, thiols, and other modifying agents, which was covered in our previous review article [9]. Alternatively, wrapping carbon particles with organic molecules [10–12] is another strategy to enhance carbon's hydrophilicity.

Surface functionalization processes are classified into two types: covalent and non-covalent processes. The present study investigates experimental procedures for the covalent functionalization of commercially available activated carbon. In the context of covalent functionalization, it is generally agreed that oxidation is typically used to pre-activate the material's surface. Compared to other pre-activation methods (e.g., direct amination of the

surface), oxidation generates superficial oxygen-containing groups. The number of these groups can be easily adjusted by controlling reaction parameters, such as the concentration of the reagents, solvents, temperature, and the duration of the reaction [13–17]. Consequently, the surface is enriched with various oxygen groups such as ketones, esters, lactones, and epoxies, as well as hydroxyl and carboxyl moieties. These groups act as "anchors" for attaching other molecules such as organosilanes onto the carbon surface [18,19].

When one knows the structure of the investigated carbon material (amorphous, crystalline, turbostratic types) [20–22] it is possible to estimate the type of oxygen groups that will dominate after an oxidative pre-activation. It is generally accepted that the higher the order in the structure and the greater the distance between graphitic planes, the more epoxy and hydroxyl groups will be present, since these groups are generated on the position of the graphene layer's basal planes. On the contrary, larger groups such as carboxyl groups require more space, so these groups will appear on the edges of the graphitic planes, characteristic of the materials with lower orders and lower distances between graphene layers [23–26]. It is critical to identify these properties to apply the appropriate surface treatments. In general, the oxygen groups' presence in the carbon structure breaks down van der Waals interactions between graphene layers, facilitating access to single graphene layers.

Other well-known methods such as exfoliation [27,28] and mechanochemical functionalization are also applied, but the present contribution focuses on oxidation as the most widely used method of pre-activating carbon surfaces. The oxidative treatments can be performed either as wet oxidation (i.e., in the liquid phase) which considers the use of acids and bases (e.g., H_2SO_4, HNO_3, H_2O_2, NaOH, and KOH) or as dry oxidation, where oxygen species on the surface are created from gasses excited by high power (i.e., plasma-assisted modification [29–31], corona discharge [7,32,33], direct ozonation [34,35], and others). One of the most frequently used wet oxidation methods for carbon is a procedure developed by Hummers and Offeman [36] to produce graphene oxide from graphite. Over time, it has become the "basic recipe" in chemistry when dealing with graphitic structures. The procedure has undergone alterations, concerning different requests for materials and experimentation [37–39].

Other examples of the successful oxidation of carbon are methods performed in autoclaves as sealed reactors, where better temperature regulation and the application of high pressures are possible. Concerning the latter, oxidation in autoclaves can also be performed as hydrothermal and solvothermal oxidation [13–17,40,41]. In hydrothermal oxidation, the main reagent is water, and other solvents are used in solvothermal reactions. The main advantage of these chemistries is the easy manipulation of temperatures (200–500 °C) and the application of pressures up to the critical point of the solvent.

The next step in the sequential functionalization of carbon is the attachment of the secondary molecules which can also serve as agents for covalent coupling. Organosilanes, for example, are bonded to carbon via hydroxy groups at the carbon surface, and the organosilane's terminating groups (e.g., glycidyl or amino groups) are compatible with and reactive towards epoxy and polyurethane resins. The silanization of carbon surfaces has been studied for carbon nanotubes, carbon fibers, activated carbon [8,18,42–48], and other materials, demonstrating that this method can be utilized for adapting the surface properties of carbon. Other functionalities attached in secondary reactions (e.g., amines, amides, and thiols) are important to enhance the hydrophilicity of the carbon surface. It is also worth noting that surface functionalization is not restricted to oxidation as a necessary pre-activation step. It can also be performed via cycloadditions ([4 + 2] (Diels–Alder), [3 + 2], and [2 + 1] additions) [9,49–51], radical reactions, and other pathways.

The major aim of this study was to investigate the sequential functionalization of activated carbon derived from coconut shells. This type of activated carbon was chosen as a model compound due to its high surface-to-volume ratio and narrow particle size distribution. To functionalize CSC, the carbon surface was pre-activated either via solvothermal oxidation with nitric acid (HNO_3) or by plasma-assisted oxidation with Ar and O_2. A further step in changing surface chemistry was performed when C=O groups were re-

duced to OH groups with lithium aluminum hydride (LiAlH$_4$) and then functionalized with 3-(aminopropyl)trimethoxysilane (APTMS) or (3-glycidyloxypropyl)trimethoxysilane, respectively. The functionalization improves carbon's suitability for application as a filler in polymeric materials.

Some of the common analytical methods that can be used in determining the properties of functionalized carbon and its surface are solid-state nuclear magnetic resonance spectroscopy (ss-NMR), inverse gas chromatography (IGC), and mass spectroscopic techniques such as TOF-SIMS (MS) as well as infrared spectroscopy (ATR-FTIR) and Raman spectroscopy. X-ray photoelectron spectroscopy (XPS) and scanning electron microscopy (SEM) are applied as element-sensitive surface analytical techniques. The most significant advantage of ss-NMR is that it yields detailed structural information about the chemical structure of the functionalized material [52]. IGC, on the other hand, is a versatile approach for investigating a wide range of materials, including powders and fibers, to assess properties like surface energy, acid–base characteristics, and surface heterogeneity [53]. Mass spectroscopic techniques such as TOF-SIMS [54] are often used in trace analysis, but are particularly useful for establishing precise molecular structures, esp. in surface analysis. Infrared and Raman techniques are convenient techniques to assess the presence of functional groups but are less surface sensitive (except tip-enhanced methods such as TERS). On the other hand, XPS is extremely surface sensitive and reveals both elemental composition and chemical states, with a depth of analysis of 5 – 10 nm. SEM gives high-resolution 3D images of sample surfaces, showing precise details of sample morphology. In combination with EDX spectroscopy (SEM-EDX), the elemental composition of materials can be obtained with high lateral resolution. Regarding the porosity of carbonaceous materials, gas sorption measurements and BET analysis are commonly employed to assess specific surface area, pore volume, and pore size [55,56].

Given the variety of methods available for determining the properties of functionalized carbon, we chose ATR-FTIR and XPS to investigate changes in surface composition and SEM to assess potential morphological changes.

2. Materials and Methods

2.1. Chemicals and Instruments

In this study, activated carbon (coconut shell carbon (CSC) YP-80F from Kuraray, Tokyo, Japan) was applied. According to the manufacturer's information, this CSC has a surface area of 2212.5 m^2/g, a total pore volume of 0.61 cm^3/g, and an average pore size of 23.04 Å. The particle diameter distribution is characterized as follows: 1.9 μm (D10); 5.6 μm (D50); 9.8 μm (D90). A diluted solution of HNO$_3$ (65 %, Carl Roth, Karlsruhe, Germany) was used for wet oxidation of the carbon in autoclave reactions. The stainless steel vertical autoclave (100 mL) was equipped with a heating jacket and a magnetic stirring unit purchased from Carl Roth GmbH (Karlsruhe, Germany). The plasma reactor (Tetra 100 LF PC, low-pressure plasma device, Diener, Ebhausen, Germany) with a maximum power of 1000 W and frequency of 80 kHz was used in the dry oxidation method with argon (99.9%, Linde, Stadl-Paura, Austria) and oxygen (99.9 %, Linde, Austria). The oxidized carbons were reduced using LiAlH$_4$ (1.0 M LiAlH$_4$ solution in THF, from Sigma Aldrich, Schnelldorf, Germany) and concentrated (96 %) H$_2$SO$_4$ from Carl Roth GmbH (Karlsruhe, Germany). Secondary functionalization was accomplished by silanization with 3-(aminopropyl)trimethoxysilane (97 %, from Sigma Aldrich, Schnelldorf, Germany) and (3-glycidyloxypropyl)trimethoxysilane (97 %, from Sigma Aldrich, Schnelldorf, Germany) in ethanol (99.9 %, from AustrAlco, Spillern, Austria) with acetic acid ($\geq$ 99.7%, from Sigma Aldrich, Schnelldorf, Germany) as a catalyst.

2.2. Characterization Methods

ATR-FTIR spectra of pristine, oxidized, APTMS- and GPTMS-modified CSC were collected with an FTIR spectrometer (Bruker Vertex, from Bruker Corp., Billerica, Massachusetts, USA) equipped with a single-reflection ATR unit (spectral range from 400 to

4000 cm^{-1}, resolution 1 cm^{-1}, 32 scans). The spectra of thoroughly dried CSC samples were obtained by placing a small amount of CSC powder onto the diamond crystal of the ATR unit.

The chemical composition of the sample surfaces was determined by X-ray photo-electron spectroscopy (XPS) using a ThermoFisher Scientific Nexsa G2 Surface Analysis System (Waltham, Massachusetts, USA) with monochromatic Al K-α radiation. Survey scans were performed with a pass energy of 200 eV and an energy resolution of 1.0 eV, whereas high-resolution spectra were taken with a pass energy of 50 eV and a resolution of 0.1 eV. The C1s line at 284.8 eV was used to calibrate the binding energy scale for the experiments. In the calculation of the surface composition, hydrogen was omitted. At least two measurements were performed for each sample. The deconvolution of XPS signals was performed with the software CasaXPS (Version 165 2.3.26). In these XPS studies, the Shirley function was used for background subtraction. The peak fitting for C-C/C=C in the C1s spectra incorporated an asymmetric line-shape model, specifically the A(a,b,n)GL(p) function. This model combines the Gaussian/Lorentzian product formula with an asymmetric modification to represent these peaks better. For other groups in C1s spectra (i.e., C-O, C=O and O-C=O), the GL(p) model employed the standard Gaussian/Lorentzian product formula.

The surface morphology of functionalized materials was studied using a scanning electron microscope (FE-SEM TESCAN Clara instrument from Oxford Instruments, Abingdon, UK). CSC samples were uniformly placed on a metal holder before being sputtered with an ultrathin coating of gold.

2.3. Sequential Surface Modification of Carbon

The CSC's surface was sequentially modified in three process steps. First, wet or dry oxidation (pre-activation) followed by reduction with $LiAlH_4$ and secondary functionalization was carried out. Wet oxidation was carried out in 1 M HNO_3 (prepared from 65% HNO_3). Dry oxidation was performed in a plasma reactor using a rotary electrode and a mixture of argon and oxygen. It was observed that the silanization of only oxidized samples is not possible as only oxidized samples lack the -OH groups necessary for the coupling reaction with the organosilanes. Therefore, to improve the coupling of APTMS and GPTMS onto oxidized CSC, the oxidized carbon was treated with $LiAlH_4$ to transform superficial carbonyl species into hydroxyl groups. As the used carbon is defined as turbostratic, the above-described mechanism of introducing oxygen groups to the carbon particles can be applied.

2.3.1. Oxidation (Pre-Activation)
Solvothermal Oxidation with HNO_3

Solvothermal oxidation, representative of the wet oxidation of CSC, was executed in a temperature range from 100 °C to 250 °C. Preliminary experiments were performed in glass vials under atmospheric conditions (pressureless) for 6 h. Since reactions in an autoclave are known to reduce reaction time, all further oxidation reactions were performed in an autoclave for 2 h. In these experiments, a ratio of 100 mg of CSC to 10 mL of 1 M HNO_3 was consistently maintained. Before the oxidation reaction, the prepared mixture was sonicated for 60 min to achieve a complete dispersion of CSC. Two hours of continuous stirring and heating in the autoclave followed (120 °C); after that, the reaction solution was filtered (vacuum filtration). The oxidized CSC samples were washed with distilled with water until the pH was 7, collected, and dried in an oven at a temperature of 110 °C overnight.

Plasma Oxidation

Dry oxidation was carried out in a low-temperature plasma reactor (Tetra 100 LF PC, Diener, Ebhausen, Germany) using a rotary electrode (the speed was kept at 80 %). Dry oxidation was carried out in two steps [57]. Before the treatment, the chamber was evacuated to a base pressure (p) of 0.1 mbar. The initial step included the so-called "etching"

of the CSC. In this treatment, the power of the rotary cathode was set to 100 W, under a continuous supply of Ar (30 sccm) for 10 min, resulting in a pressure of 0.25 mbar. Immediately afterwards, an additional 100 sccm of O_2 was introduced, and the treatment with this mixture of Ar and O_2 was carried out with 900 W for 20 min. When the ratio of gasses was 77 % (O_2) to 23 % (Ar), the total pressure was set to 0.35 mbar. By the end of the treatment, the chamber was vented with air, and the sample was collected and stored in a glass vial.

2.3.2. Reduction in Oxidized Carbon with LiAlH$_4$

Oxidative treatments are generally used to provide a surface with various oxygen groups. According to our observations, wet oxidation with acids and bases results in the generation of both carbonyl (C=O) and hydroxyl groups (-OH), while dry oxidation results in a high concentration of C=O species present on the carbon surface. This is due to the exposition of the carbon to only the Ar and O_2 environment during the plasma treatment. To convert carbonyl groups into the desired hydroxyl groups, LiAlH$_4$ was used as a strong reducing agent for C=O groups [8,58,59]. Then, 100 mg of wet- and dry-oxidized CSC was added to a 10 mL solution of LiAlH$_4$ in dry THF (0.1M) and stirred continuously at room temperature for 60 min. After the reaction, the material was centrifuged and re-dispersed in 9 mL of THF, to which 1 mL of HCl was added dropwise while slowly stirring for 30 min (removal of excess LiAlH$_4$). The CSC was separated by centrifugation, washed with THF three times, and finally dried at 110 °C overnight.

2.3.3. Coupling of 3-(Aminopropyl)ltrimethoxysilane (APTMS) and 3-(Glycidoxypropyl)trimethoxysilane (GPTMS)

In preliminary experiments, silanization was performed in three different solvents: ethanol, acetone, and toluene. The silanization in acetone resulted in coagulation, while silanization in toluene led to the deposition of the CSC particles in leaflets [8,18,60–62]. As our initial aim was to preserve the powder form, these approaches were not further pursued. Instead, the coupling of APTMS and GPTMS was accomplished in ethanol solution (EtOH (aq)) [63]. In the present work, silanization was carried out in an autoclave to avoid EtOH evaporation at higher temperatures. The reaction solution was prepared in a glass vial to prevent contamination. For the functionalization of wet-oxidized CSC, 10 mL of a water/ethanol mixture (1:1 by weight), carbon (100 mg), and organosilane (100 μL) were added, along with 10 μL of acetic acid as a catalyst [64]. Contrary to this, for dry-oxidized carbon, the reaction was performed in water (without ethanol), since it was observed that organosilanes are more prone to couple with dry-oxidized and reduced carbon in aqueous solution. After 60 min of sonication, the glass vial was placed in the autoclave. The silanization reaction was conducted at 80 °C for 6 h. After cooling to room temperature, the reaction mixture was centrifuged, and the collected CSC was washed multiple times with distilled water. The modified CSC was finally dried at 110 °C overnight.

3. Results and Discussion

3.1. Attenuated Total Reflectance Spectroscopy (ATR-FTIR)

3.1.1. Investigation of Pristine, Oxidized, and Reduced CSC

The FTIR-ATR spectra were used to reveal qualitative but not quantitative changes in the surface composition by evaluation of the presence/absence of specific bands. When altering the surface chemistry of CSC by a wet pre-activation process, it was found that the introduction of hydroxyl groups presented a challenge when methods described in the literature were applied. The ATR-FTIR spectrum of pristine CSC, as shown in Figure 1, reveals the following signals: (i) -OH groups at wavenumbers higher than 3000 cm^{-1}; (ii) asymmetric CH$_2$ vibrations of hydrocarbon units, which are linked to the disrupted graphene lattice in turbostratic carbon, at a position around 2968 cm^{-1}, as well as C=C-H signals at wavenumbers higher than 3000 cm^{-1}; (iii) C=O vibrations with peaks at 1740 cm^{-1} and 1700 cm^{-1} (correlated to lactones, ketones, and aldehydes, and carboxylic acids, re-

spectively); and (iv) two signals at 1216 cm^{-1} and 1366 cm^{-1} which can be attributed to C–O–C groups, e.g., in aromatic ethers, epoxy groups, and lactones. An additional signal at 918 cm^{-1} is attributed to the ring vibration of epoxides [19,60,65–67]. All of this suggests that the surface of pristine CSC already contains various oxygen groups. To enrich the surface with additional oxygen moieties, further oxidation and reduction procedures were carried out. As can be seen in Figure 1B, no additional peaks were observed after oxidation with HNO$_3$. However, quantitative changes in the oxygen-containing groups are suggested and were further investigated by XPS (see Section 3.2.).
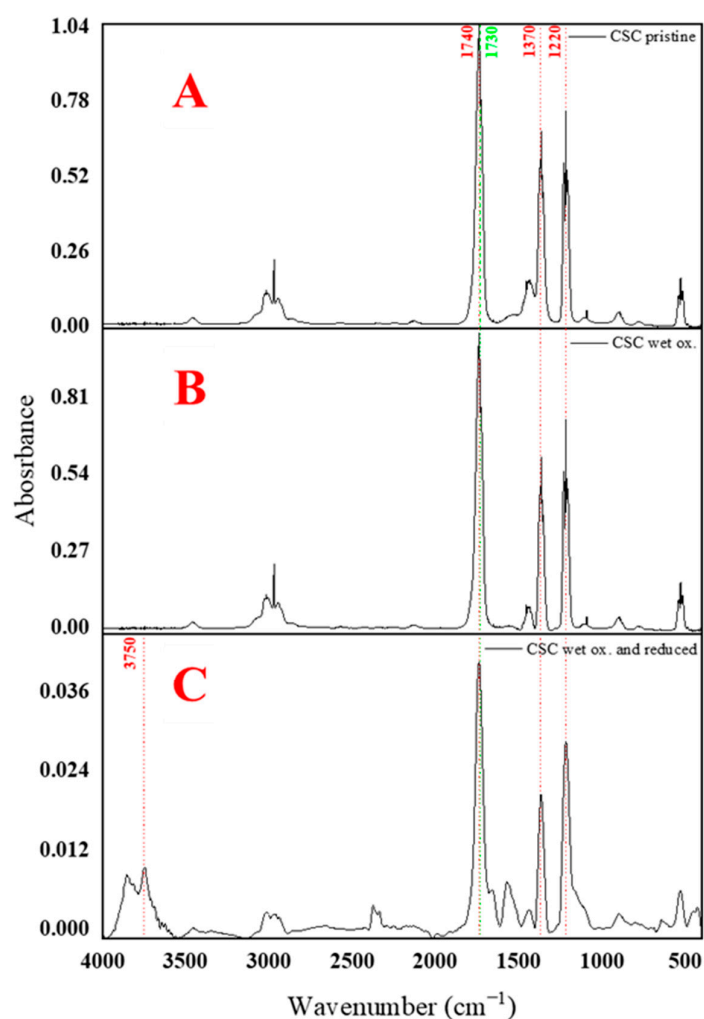

Figure 1. ATR-FTIR spectra of pristine (**A**), HNO$_3$-oxidized (**B**), and LiAlH$_4$-reduced CSC (**C**) with specific wavenumbers of C=O groups (1740 and 1730 cm^{-1}), C-O, and -OH (1370 cm^{-1} and 1220 cm^{-1}), as well as -OH groups (3750 cm^{-1}).

Reduction with LiAlH$_4$ is a well-known technique that is employed to reduce complex chemical groups to desired functionalities with lower oxidation levels, e.g., carbonyl groups to hydroxyl groups. The reduction was performed after the solvothermal oxidation of CSC with HNO$_3$ to generate additional hydroxyl groups. This was proven by the strong and broad signal emerging at 3740 cm^{-1} in the FTIR spectrum (Figure 1C) which is attributed to -OH groups. However, it should be noted that this -OH signal is found at an unusually high wavenumber (>3500 cm^{-1}). Nevertheless, this signal indicates a generation of hydroxyl groups in CSC as a result of the partial reduction of carbonyl groups. The apparent invariance of the carbonyl signal (1740 and 1730 cm^{-1}) during the oxidation and reduction processes may be explained by the fact that the analytical depth of ATR-FTIR measurements

is far higher than the layer thickness affected by oxidative treatments. On the other hand, the idea that wet chemical reactions also take place inside the pores of CSC cannot be ruled out.

For plasma-oxidized carbon, no significant changes were detectable from ATR-FTIR spectra. ATR-FTIR is too insensitive to detect changes in the top atomic layers of CSC. To sum up, ATR-FTIR spectroscopy provided limited and only qualitative information on chemical changes at the CSC's surface.

3.1.2. Investigation of CSC Functionalized with Organosilanes

After the reaction of reduced CSC with organosilanes (i.e., APTMS and GPTMS) the FTIR spectra displayed additional signals (see Figure 2). A characteristic new signal typical of Si-O-C units [19,60,66] was detected in the spectral range from 998 to 1048 cm^{-1}. These spectral changes are characteristic of coupled organosilanes and appeared both for wet- and plasma-activated CSCs. In Figure 2B,D, a weak signal at 918 cm^{-1} is discernible, which indicates the presence of oxirane groups after the coupling of the GPTMS [68–70].
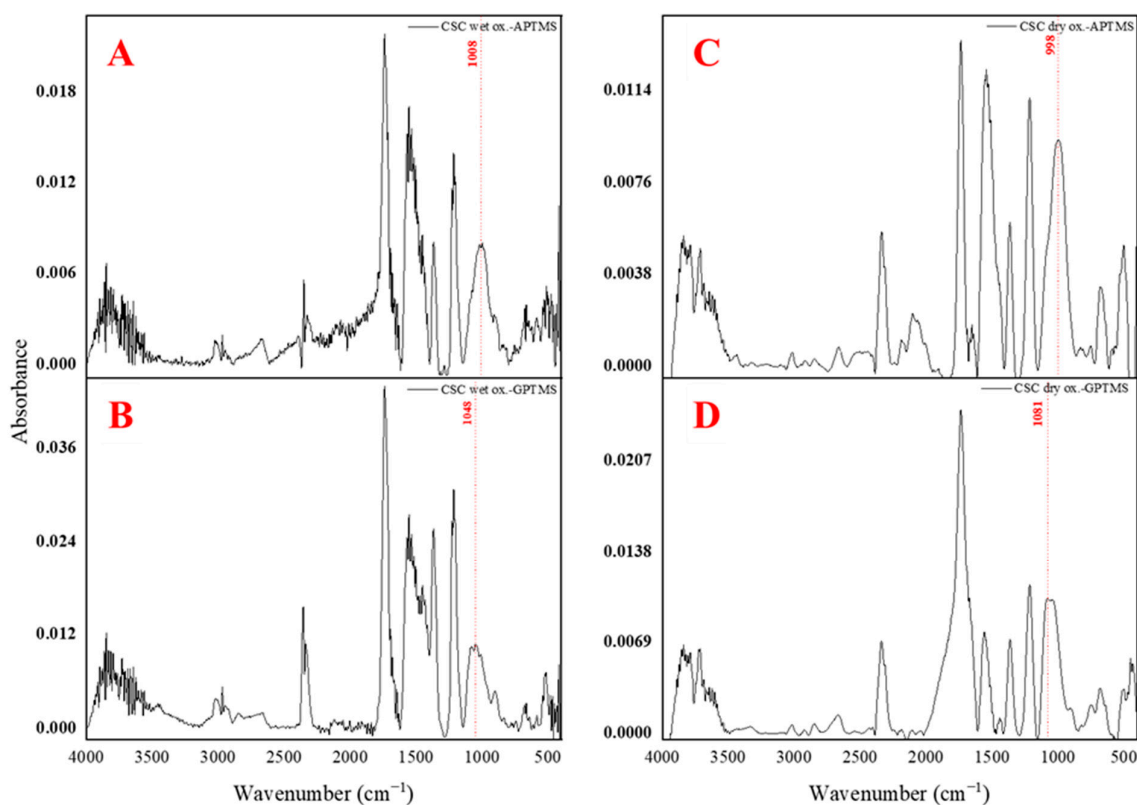

Figure 2. ATR-FTIR spectra of (**A**) wet-oxidized CSC functionalized with APTMS, (**B**) wet-oxidized CSC functionalized with GPTMS, (**C**) dry-oxidized CSC functionalized with APTMS, and (**D**) dry-oxidized CSC functionalized with GPTMS. The signal marked in red is characteristic of Si-O-C units. An additional Si-O-C bond can be found within the range of 998 cm^{-1} to 1081 cm^{-1} for samples A-D.

According to our observation that Si-O-C peaks were well discernible by ATR-FTIR spectroscopy but that XPS indicated only extremely thin organosilane layers at the outer surface of CSC (vide infra), it may be concluded that reactions of organosilanes also occur in the pores of CSC. APTMS and GPTMS molecules have a length of approx. 5 Å and 8 Å, respectively [71,72]. These molecules are smaller than the average pore diameter in CSC (23 Å) and suitable for adsorption and absorption processes due to the large surface area of CSC (>2200 m^2/g) [73]. Condensation and coupling reactions of organosilanes inside the pores could explain the FTIR results. The enhanced chemisorption of APTMS, GPTMS, and other organosilanes in porous carbons has been reported in the literature (see the

comprehensive review [74]). Also, the influence of, e.g., heteroatom (nitrogen)-doped pores on adsorption and precise chemical reaction equilibria inside carbon pores has been studied in detail, including using Monte-Carlo methods [57,75]. Various methods for the chemical activation of nano- and mesopores of carbon with, e.g., $FeCl_3$ [76] have been reported.

3.2. X-Ray Photoelectron Spectroscopy (XPS)

Compared to FTIR spectroscopy, XPS is better suited to detect changes at surfaces as the depth of analysis in XPS amounts to approximately 5 nm. The results of XPS analyses are compiled in Tables 1 and 2. The individual peak positions of C1s obtained from HNO_3-oxidized and $LiAlH_4$-reduced CSCs are consistent with the literature [19,77,78].

Table 1. Surface composition of pristine, oxidized, reduced, and APTMS/GPTMS-functionalized CSCs.

Sample	at. % C	at. % O	ratio O/C	at. % N	at. % Si	at. % Cl	at. % Al
CSC pristine	94.4	5.6	0.1	-	-	-	-
CSC wet ox.	84.1	15.0	0.1	0.9	-	-	-
CSC dry ox.	77.4	22.6	0.3	-	-	-	-
CSC wet ox.-reduced	85.1	13.0	0.2	-	-	1.9	-
CSC dry ox.-reduced	81.7	16.3	0.2	-	-	2.0	-
CSC wet ox. -APTMS	75.4	17.6	0.2	3.9	3.2	-	-
CSC wet ox.-GPTMS	79.1	17.4	0.2	-	1.9	0.7	-
CSC dry ox.-APTMS	78.3	19.9	0.3	4.8	5.1	-	1.9
CSC dry ox.-GPTMS	73.9	21.8	0.3	-	2.8	0.7	0.8

Table 2. The characteristic position of the C1s signal for different carbon-based functional groups [19,77,78], and relative atomic percentages of these groups at the surface of pristine and modified CSC.

Group	C-Si	C=C/C-C	C-N	C-O	C=O	O-C=O	C-O/(C=O + O-C=O)
	C1s binding energies of functional groups						
Binding energy (eV)	283.33–283.37	284.40–284.60	285.64	285.93–286.6	287.00–288.69	289.05–289.45	
	Atomic percentage of functional groups						
CSC pristine	-	89.3	-	6.4	4.4	-	1.5
CSC wet ox.	-	78.2	-	12.1	9.7	-	1.3
CSC dry ox.	-	49.0	-	25.9	13.0	12.1	1.0
CSC wet ox.-reduced	-	64.0	-	15.2	13.1	7.8	0.7
CSC dry ox.-reduced	-	67.0	-	14.1	11.5	7.5	0.8
CSC wet ox. -APTMS	1.0	76.3	1.2	11.4	6.9	3.3	1.1
CSC wet ox.-GPTMS	0.5	69.2	-	16.2	8.5	5.6	1.1
CSC dry ox. APTMS	2.4	55.4	3.0	28.5	5.3	5.5	2.6
CSC dry ox.-GPTMS	1.4	58.4	-	28.7	8.00	3.5	2.5

Table 1 presents the atomic composition of pristine, oxidized, reduced, and APTMS/GPTMS-functionalized CSCs. The increase in the oxygen content from 5.6 at. % (pristine CSC) to 15.0 at. % indicated the successful oxidation of CSC by the solvothermal method. The small amount of nitrogen (0.9 at. %) can be attributed to the formation of nitro groups ($R-NO_2$) as well as nitrates ($R-O-NO_2$) on carbon, which have also been reported in the literature [79]. A large amount of oxygen was also detected for dry-oxidized samples (22.6 at. %) directly after the plasma treatment, resulting in an O:C ratio of 0.3:1.

As a result of the reduction with $LiAlH_4$, where oxygen groups are transformed from C=O to C-O-C or -OH, a slight decrease in the oxygen content from 15.0 at. % to 13.0 at. % was found for the wet-oxidized CSC. This can be a result of the reduction in nitrate groups $R-O-NO_2$ at the carbon surface, which would lead to a depletion in the oxygen content. The presence of Cl is attributed to residues after working up the $LiAlH_4$-treated CSC samples with aqueous HCl. Moreover, a depletion in the oxygen content (from 22.6 at. % to 16.3 at. %) was also found for the dry-oxidized CSC reduced with $LiAlH_4$.

The successful coupling of organosilanes is evidenced by the detected amount of Si at the surface of CSC. XPS data show 3.2 at.% and 5.1 at.% Si after functionalization with APTMS for wet-oxidized and dry-oxidized CSC, respectively, and 1.9 at.% and 2.8 at.% Si

after functionalization with GPTMS for wet-oxidized and dry-oxidized CSC, respectively (see Table 1). After a reaction with APTMS, nitrogen content of 3.9 at. % was found, which was close to the Si content (3.2 at. %). Since for APTMS molecules, an atomic ratio of N:Si of 1:1 is expected, these results confirm the formation of a thin layer of APTMS on the CSC surface. As a result of functionalization with APTMS and GPTMS, the oxygen content of the surface increased from 13.0 at. % to 17.4 at. % in the case of wet-oxidized CSC and from 16.3 at. % to 19.9 at. % for dry-oxidized CSC.

This surface composition significantly differs from that which is expected for an organosilica layer with the theoretical composition of $[R-SiO_{1.5}]_n$. This indicates that mono- and oligolayers of organosilanes with thicknesses less than 5 nm [76,80–82] have been formed. In this case, a dominant contribution from the CSC substrate to the overall C1s signal can be expected.

When materials' surfaces are functionalized, the formation of self-assembled mono-layers (SAMs) is highly desirable as it provides uniformity and thus control over the well-ordered surface, easier secondary functionalization and modification, as well as stable covalent bonding with the substrate [83,84]. Whilst SAMs have been described for thiols on metal surfaces and organophosphonates on oxidic surfaces, the reaction of organosi-lanes with oxidic (and oxidized) surfaces can lead to complex and crosslinked oligo- and multi-layers, depending on the reaction conditions.

Furthermore, peak deconvolution was executed to give a more precise view of the bind-ing states of the elements present at the CSC surface. In the following, the discussion of XPS detail spectra will be limited to the C1s signals and their deconvoluted components (ranging from 283 eV to 289eV). Detailed C1s spectra of the individual CSC specimens are presented in Figure 3. Several key peaks are distinguished in the fitted and stacked components of C1s spectra of, e.g., wet- and dry-oxidized and LiAlH$_4$-reduced CSC: C=C/C-C (284.4–284.6 eV), C-O (285.9–286.6 eV), C=O (287.0–288.7 eV), and O-C=O (289.1–289.5 eV) [19,65,77,78].

Table 2 summarizes the results. According to the C1s signal of pristine CSC, 89.3 at.% C=C/C-C, 6.4 at.% C-O, and 4.4 at.% C=O are found, which is in good agreement with the literature [77,85,86]. It is presumed that C=C and C-C bonds result not only from the carbon in the aromatic plane but also from defective areas containing alkyl chains (out of plane) (see Section 2.3.). The presence of C-O and C=O units also corroborates the findings from FTIR spectroscopy, which showed C-O signals (e.g., epoxide units) as well as carbonyl signals (e.g., ketones).

After wet oxidation with HNO$_3$, the C=C/C-C groups decreased from 89.3 at.% to 78.0 at.%, which indicates their conversion to groups containing oxygen. Indeed, the C-O and C=O units increased to 12.1 at. % and 9.7 at.%, respectively. Similarly, the plasma-oxidized samples displayed a decrease in C=C/C-C bonds from 89.3 to 49.0 at.%. The concomitant increase in carbon–oxygen entities to a total value of 51.0 at.% highlights the plasma treatment as an effective surface oxidation method.

After the reduction in oxidized CSC with LiAlH$_4$, further changes in the content of C-O and C=O units were found; see Table 2. From Figure 3, it is apparent that both plasma-oxidized CSC and CSC which had been wet-oxidized and treated with LiAlH$_4$ contained large fractions of C-O units. However, the quantitative data in Table 2 show a complex situation that is difficult to interpret. It is interesting to see that, after reduction, the surface composition of both wet- and dry-oxidized CSC was similar.
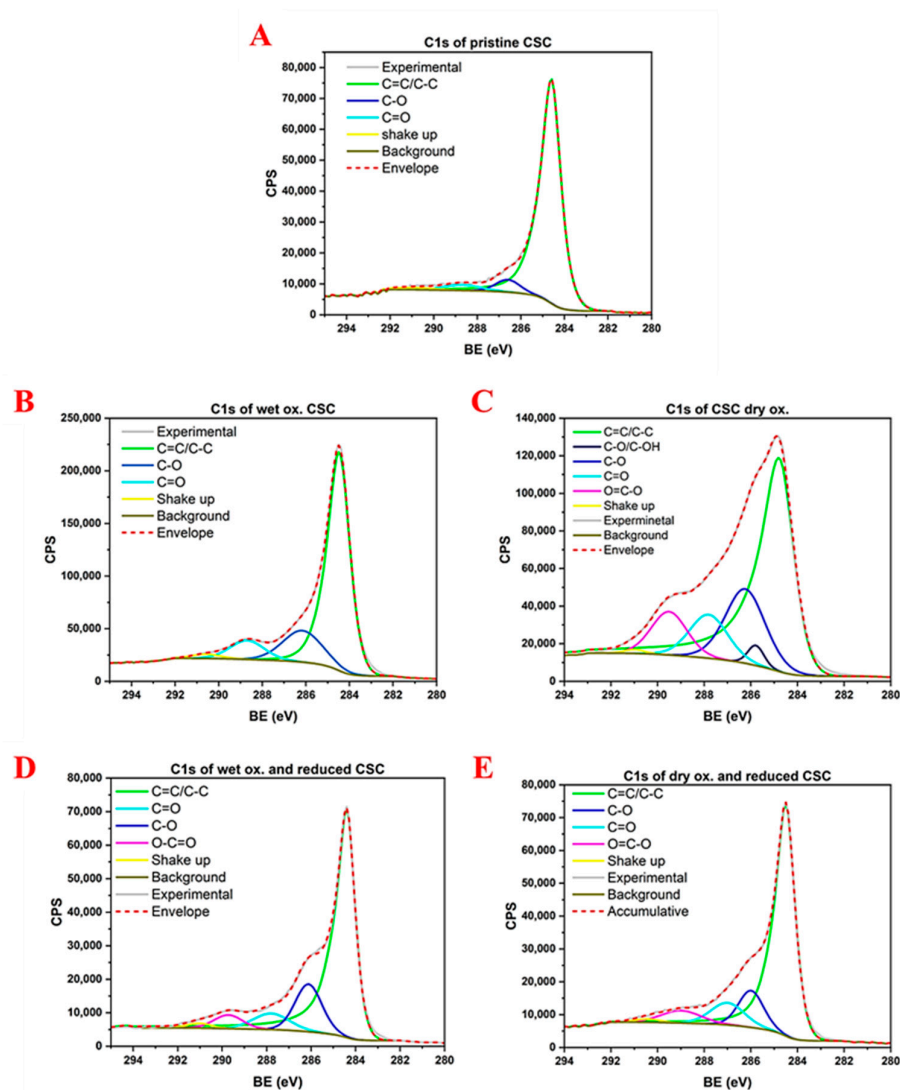
Figure 3. Detailed C1s XPS spectra for pristine (**A**), wet-oxidized (**B**), dry-oxidized (**C**) wet-oxidized and reduced with $LiAlH_4$ (**D**), and dry-oxidized and reduced with $LiAlH_4$ (**E**).

Figure 4 presents the deconvoluted C1s spectra of CSC functionalized with GPTMS and APTMS. Quantitative data (Table 2) show the presence of C-Si and C-N bonds, which proves that the surface of functionalized carbons contains organosilane units. This is in good agreement with the data on elemental surface composition (see Table 1). Especially for CSC samples that have been plasma-oxidized and then treated with $LiAlH_4$, it is evident that the attachment of GPTMS and APTMS led to a further increase in the content of C-O units (from 14 to approx. 28 %; see Table 2). This is in good agreement with the data on elemental surface composition (Table 1): the overall oxygen content of the CSC surface increased significantly after the attachment of the organosilanes, both for wet- and plasma-oxidized CSC. The generation of C-O-Si units during the coupling (i.e., condensation) reaction of the trialkoxysilanes with the surface readily explains this finding.
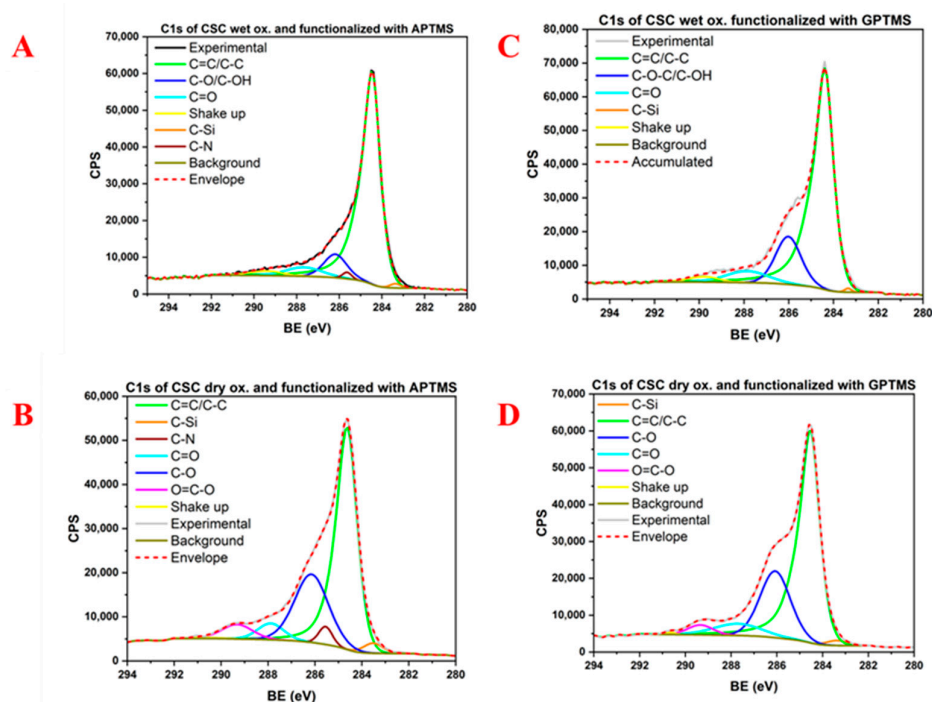
Figure 4. Detailed C1s XPS spectra for wet-oxidized CSC (**A**,**B**) and dry-oxidized CSC (**C**,**D**) after functionalization with APTMS and GPTMS, respectively.

From the data in Table 1 (Si content of the surface) and Table 2 (fraction of C-Si units), it is apparent that APTMS is more readily coupled to the surface than GPTMS, giving approx. double the amount of APTMS when compared to GPTMS. This is observed both for wet- and dry-oxidized CSC. It can also be seen that the dry oxidation of CSC leads to larger amounts of coupled organosilanes when compared to CSC oxidized with HNO_3.

As an additional study, the stability of dry-oxidized samples was monitored for a sample treated with 900 W for 20 min to determine how long plasma-activated carbon will keep the generated oxygen functionalities (hydrophilicity). The stability test was conducted over four weeks under air; see Figure 5. The steady surface composition (C and O) during storage demonstrates that the generated oxygen functionalities are highly stable and therefore resistant to losses in oxygen content on the surface over time (hydrophobic recovery).
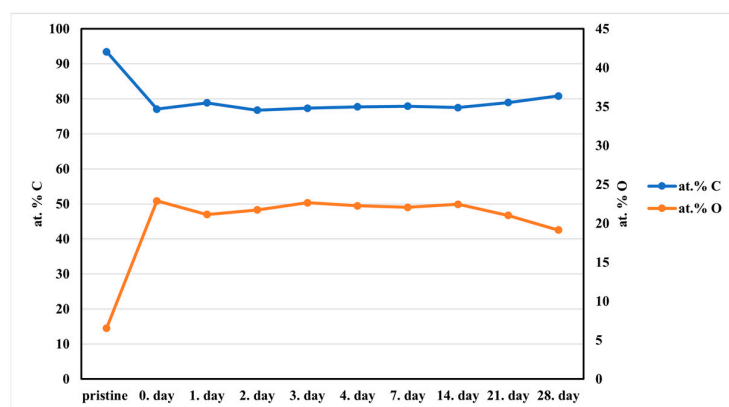

Figure 5. Surface composition of CSC after oxidative plasma treatment at 900 W for 20 min, with the sample stored under air for four weeks at room temperature.

3.3. Scanning Electron Microscopy (SEM)

SEM investigations revealed that in CSC functionalization, the available surfaces are agglomerates of particles of various sizes and shapes (see Figure 6). As a result, all performed functionalizations are suggested to occur on the surface of activated carbon particles (agglomerates). It was investigated by SEM whether CSC oxidation and further treatments would exert an influence on the shape and morphology of CSC. Figure 6 presents SEM images of CSC at different stages of activation and functionalization. As can be seen, both the oxidation and reduction processes did not significantly alter the morphology of CSC samples. Even after functionalization with APTMS or GPTMS, the morphology remained mostly unaltered. The main finding is related to the decrease in the number of cracks on the surface, which is the result of smoothening the surface due to the silane attachment. Also, this finding suggests that the treatment of CSC with organosilanes (APTMS and GPTMS) did not lead to the deposition of thick layers but rather resulted in molecular organosilane layers at the surface of CSC. This corroborates the results from XPS, which indicated a very thin coverage of CSC with mono- and/or oligolayers of organosilanes (max. 5 at.% of Si detectable by XPS).
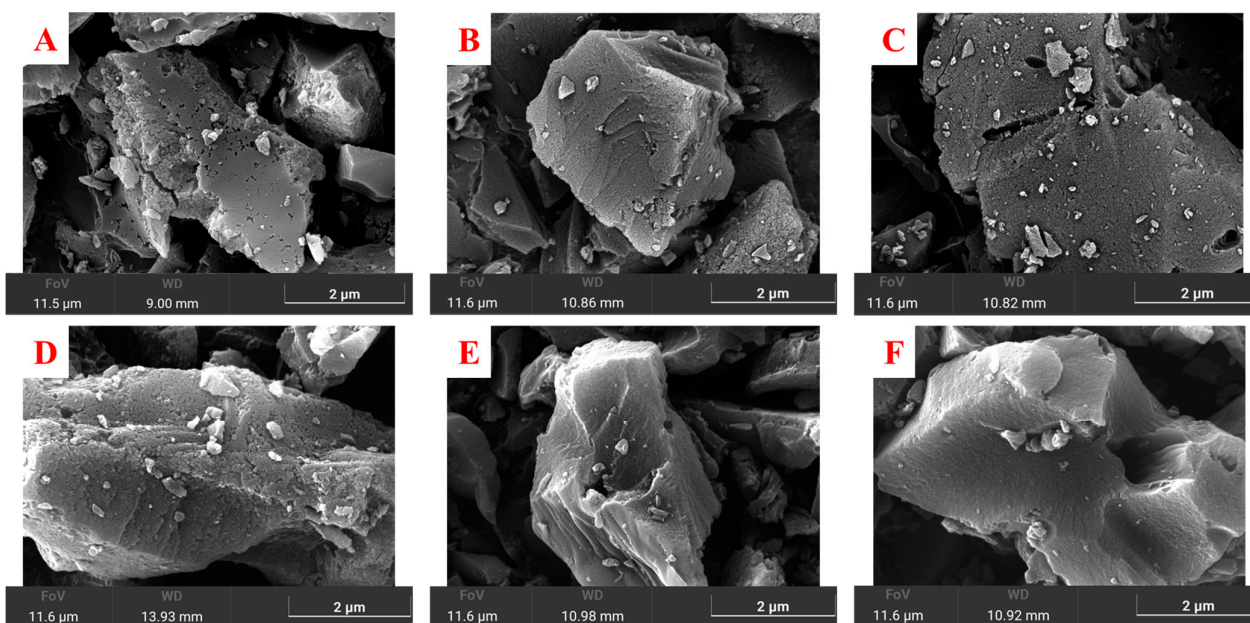

Figure 6. SEM images of pristine and modified CSC: (**A**) pristine, (**B**) wet-oxidized, (**C**) dry-oxidized, (**D**) reduced, (**E**) after coupling of APTMS, and (**F**) after coupling of GPTMS.

4. Conclusions

XPS demonstrated that two-step plasma oxidation with argon and oxygen resulted in the highest possible oxygen content of the surface (approx. 25 at. %, according to elemental composition). Regarding wet chemical oxidation with HNO_3, a solvothermal process in an autoclave is beneficial because it enables reasonable reaction times (2 h) when compared to pressureless procedures. Plasma-assisted techniques for carbon oxidation benefit from short reaction times (in our case, 30 min), a clean setup without the use of aggressive reagents, and the good stability of the oxidized surfaces (up to four weeks under ambient conditions). In our approach, the application of a reduction step (using $LiAlH_4$) proved advantageous to obtain a better-defined carbon surface bearing a sufficient number of -OH units, which is a prerequisite for the reaction with organosilanes. The dry oxidation of CSC (followed by reduction with $LiAlH_4$) resulted in a larger amount of coupled organosilanes when compared to wet-oxidized and also $LiAlH_4$-reduced CSC samples. When comparing APTMS and GPTMS, it was found that APTMS is more readily coupled to the CSC surface than GPTMS. The immobilized organosilane layers were found to be very thin, probably

comprising mono- and bilayers with a thickness below 5 nm, as concluded from XPS data. To sum up, in this work, two convenient procedures have been elaborated on for the coupling of organosilanes to the surface of activated carbon.

References

1. Jaria, G.; Lourenço, M.A.O.; Silva, C.P.; Ferreira, P.; Otero, M.; Calisto, V.; Esteves, V.I. Effect of the surface functionalization of a waste-derived activated carbon on pharmaceuticals' adsorption from water. *J. Mol. Liq.* **2020**, *299*, 112098. [CrossRef]
2. Jayasinghe, S.; Pasan Siriwardena, D.; Munaweera, I.; Perera, C.; Kottegoda, N. Sustainable synthesis of highly functionalized activated carbon using plasma technology. *ChemPlusChem* **2022**, *87*, e202200202. [CrossRef] [PubMed]
3. Azhagapillai, P.; Al Shoaibi, A.; Chandrasekar, S. Surface functionalization methodologies on activated carbons and their benzene adsorption. *Carbon Lett.* **2021**, *31*, 419–426. [CrossRef]
4. He, X.; Zhu, J.; Wang, H.; Zhou, M.; Zhang, S. Surface Functionalization of Activated Carbon with Phosphonium Ionic Liquid for CO_2 Adsorption. *Coat.* **2019**, *9*, 590. [CrossRef]
5. Demiral, İ.; Samdan, C.; Demiral, H. Enrichment of the surface functional groups of activated carbon by modification method. *Surf. Interfaces* **2021**, *22*, 100873. [CrossRef]
6. Mohamed Hatta, N.S.; Hussin, F.; Gew, L.T.; Aroua, M.K. Enhancing surface functionalization of activated carbon using amino acids from natural source for CO_2 capture. *Sep. Purif. Technol.* **2023**, *313*, 123468. [CrossRef]
7. Pego, M.F.F.; Bianchi, M.L.; Carvalho, J.A.; Veiga, T.R.L.A. Surface modification of activated carbon by corona treatment. *Chem. Sci. An. Acad. Bras. Ciênc.* **2019**, *91*, e20170947. [CrossRef]
8. He, Q.; Xu, Y.; Wang, C.; She, S.; Zhou, S.; Wang, R. Silane modification and characterization of activated carbon. *Adsorption* **2012**, *18*, 23–29. [CrossRef]
9. Pustahija, L.; Kern, W. Surface Functionalization of (Pyrolytic) Carbon—An Overview. *Carbon* **2023**, *9*, 38. [CrossRef]
10. Voge, C.M.; Johns, J.; Raghavan, M.; Morris, M.D.; Stegemann, J.P. Wrapping and dispersion of multiwalled carbon nanotubes improves electrical conductivity of protein–nanotube composite biomaterials. *J. Biomed. Mater. Res. A* **2013**, *101A*, 231–238. [CrossRef]
11. Fujigaya, T.; Nakashima, N. Non-covalent polymer wrapping of carbon nanotubes and the role of wrapped polymers as functional dispersants. *Sci. Technol. Adv. Mater.* **2015**, *16*, 024802. [CrossRef] [PubMed]
12. Verma, P.; Anoop, S.; Sasidhara Rao, V.; Sharma, A.K.; Uma Rani, R. Multiwalled carbon nanotube-poly vinyl alcohol nanocomposite multifunctional coatings on aerospace alloys. *Mater. Today Proc.* **2018**, *5*, 21205–21216. [CrossRef]
13. Feng, S.-H.; Li, G.-H. Chapter 4-Hydrothermal and Solvothermal Syntheses. In *Modern Inorganic Synthetic Chemistry*, 2nd ed.; Xu, R., Xu, Y., Eds.; Elsevier: Amsterdam, The Netherlands, 2017; pp. 73–104. [CrossRef]
14. Suvaci, E.; Özel, E. Hydrothermal Synthesis. In *Encyclopedia of Materials: Technical Ceramics and Glasses*; Pomeroy, M., Ed.; Elsevier: Oxford, UK, 2021; pp. 59–68. [CrossRef]
15. Silva, A.M.T.; Machado, B.F.; Figueiredo, J.L.; Faria, J.L. Controlling the surface chemistry of carbon xerogels using HNO3-hydrothermal oxidation. *Carbon* **2009**, *47*, 1670–1679. [CrossRef]
16. Morales-Torres, S.; Silva, T.L.S.; Pastrana-Martínez, L.M.; Brandão, A.T.S.C.; Figueiredo, J.L.; Silva, A.M.T. Modification of the surface chemistry of single- and multi-walled carbon nanotubes by HNO_3 and H_2SO_4 hydrothermal oxidation for application in direct contact membrane distillation. *Phys. Chem. Chem. Phys.* **2014**, *16*, 12237–12250. [CrossRef]
17. Wang, Q.; Zhu, B.; Su, D.S. Hydrothermal method oxidized carbon nanotube: Properties and performances in epoxy composite. *Diam. Relat. Mater.* **2021**, *114*, 108321. [CrossRef]

18. Kathi, J.; Rhee, K.-Y.; Lee, J.H. Effect of chemical functionalization of multi-walled carbon nanotubes with 3-aminopropyltriethoxysilane on mechanical and morphological properties of epoxy nanocomposites. *Compos. Part A Appl. Sci. Manuf.* **2009**, *40*, 800–809. [CrossRef]

19. Lu, Y.; Li, H.; Lin, M.; Ng, W.; Liu, H. Mechanical properties of 3-glycidoxypropyltrimethoxysilane functionalized multi-walled carbon nanotubes/epoxy composites cured by electron beam irradiation. *J. Compos. Mater.* **2013**, *47*, 1685–1694. [CrossRef]

20. Bianco, A.; Cheng, H.-M.; Enoki, T.; Gogotsi, Y.; Hurt, R.H.; Koratkar, N.; Kyotani, T.; Monthioux, M.; Park, C.R.; Tascon, J.M.D.; et al. All in the graphene family—A recommended nomenclature for two-dimensional carbon materials. *Carbon* **2013**, *65*, 1–6. [CrossRef]

21. Toth, P. Nanostructure quantification of turbostratic carbon by HRTEM image analysis: State of the art, biases, sensitivity and best practices. *Carbon* **2021**, *178*, 688–707. [CrossRef]

22. Li, Z.Q.; Lu, C.J.; Xia, Z.P.; Zhou, Y.; Luo, Z. X-ray diffraction patterns of graphite and turbostratic carbon. *Carbon* **2007**, *45*, 1686–1695. [CrossRef]

23. Kovtyukhova, N.I.; Ollivier, P.J.; Martin, B.R.; Mallouk, T.E.; Chizhik, S.A.; Buzaneva, E.V.; Gorchinskiy, A.D. Layer-by-Layer Assembly of Ultrathin Composite Films from Micron-Sized Graphite Oxide Sheets and Polycations. *Chem. Mater.* **1999**, *11*, 771–778. [CrossRef]

24. Gupta, B.; Kumar, N.; Panda, K.; Kanan, V.; Joshi, S.; Visoly-Fisher, I. Role of oxygen functional groups in reduced graphene oxide for lubrication. *Sci. Rep.* **2017**, *7*, 45030. [CrossRef] [PubMed]

25. Besenhard, J.O.; Schulte, A.; Schur, K.; Jannakoudakis, P.D. Preparation of Voltammetric and Potentiometric Carbon Fibre Microelectrodes. In *Microelectrodes: Theory and Applications*; Montenegro, M.I., Queirós, M.A., Daschbach, J.L., Eds.; Springer: Dordrecht, The Netherlands, 1991; pp. 189–204. [CrossRef]

26. Hérold, A. Synthesis of graphite intercalation compounds. In *Chemical Physics of Intercalation*; Legrand, A.P., Flandrois, S., Eds.; Springer: Boston, MA, USA, 1987; pp. 3–45. [CrossRef]

27. Stankovich, S.; Dikin, D.A.; Dommett, G.H.B.; Kohlhaas, K.M.; Zimney, E.J.; Stach, E.A.; Piner, R.D.; Nguyen, S.T.; Ruoff, R.S. Graphene-based composite materials. *Nature* **2006**, *442*, 282–286. [CrossRef]

28. Huang, Z.; Chen, H.; Zhao, L.; Fang, W.; He, X.; Li, W.; Tian, P. In suit inducing electron-donating and electron-withdrawing groups in carbon nitride by one-step NH4Cl-assisted route: A strategy for high solar hydrogen production efficiency. *Environ. Int.* **2019**, *126*, 289–297. [CrossRef]

29. Zhang, Z.; Wilson, J.L.; Kitt, B.R.; Flaherty, D.W. Effects of Oxygen Plasma Treatments on Surface Functional Groups and Shear Strength of Carbon Fiber Composites. *ACS Appl. Polym. Mater.* **2021**, *3*, 986–995. [CrossRef]

30. Hosseini, H.; Ghaffarzadeh, M. Surface functionalization of carbon nanotubes via plasma discharge: A review. *Inorg. Chem. Commun.* **2022**, *138*, 109276. [CrossRef]

31. Lu, X.; Yang, X.; Tariq, M.; Li, F.; Steimecke, M.; Li, J.; Varga, A.; Bron, M.; Abel, B. Plasma-etched functionalized graphene as a metal-free electrode catalyst in solid acid fuel cells. *J. Mater. Chem. A* **2020**, *8*, 2445–2452. [CrossRef]

32. ul Haq, A.; Boyd, A.; Acheson, J.; McLaughlin, J.; Meenan, B.J. Corona Discharge-Induced Functional Surfaces of Polycarbonate and Cyclic Olefins Substrates. *Surf. Coat. Technol.* **2019**, *362*, 185–190. [CrossRef]

33. Park, S.-J.; Jin, J.-S. Effect of Corona Discharge Treatment on the Dyeability of Low-Density Polyethylene Film. *J. Colloid Interface Sci.* **2001**, *236*, 155–160. [CrossRef]

34. Razumovskii, S.D.; Gorshenev, V.N.; Kovarskii, A.L.; Kuznetsov, A.M.; Shchegolikhin, A.N. Carbon Nanostructure Reactivity: Reactions of Graphite Powders with Ozone. *Fuller. Nanotub. Carbon Nanostruct.* **2007**, *15*, 53–63. [CrossRef]

35. Mawhinney, D.B.; Yates, J.T. FTIR study of the oxidation of amorphous carbon by ozone at 300 K—Direct COOH formation. *Carbon* **2001**, *39*, 1167–1173. [CrossRef]

36. Hummers, W.S.; Offeman, R.E. Preparation of Graphitic Oxide. *J. Am. Chem. Soc.* **1958**, *80*, 1339. [CrossRef]

37. Sakib, N.; Rahman, M.M.; Ali, M.H. Optimization of the Oxidation Temperature of Graphene Oxide. *Int. J. Eng. Res. Technol.* **2019**, *8*, 736–739. [CrossRef]

38. Marcano, D.C.; Kosynkin, D.V.; Berlin, J.M.; Sinitskii, A.; Sun, Z.; Slesarev, A.; Alemany, L.B.; Lu, W.; Tour, J.M. Improved Synthesis of Graphene Oxide. *ACS Nano* **2010**, *4*, 4806–4814. [CrossRef]

39. Gupta, V.; Sharma, N.; Singh, U.; Arif, M.; Singh, A. Higher oxidation level in graphene oxide. *Optik* **2017**, *143*, 115–124. [CrossRef]

40. Marques, R.R.N.; Machado, B.F.; Faria, J.L.; Silva, A.M.T. Controlled generation of oxygen functionalities on the surface of Single-Walled Carbon Nanotubes by HNO$_3$ hydrothermal oxidation. *Carbon* **2010**, *48*, 1515–1523. [CrossRef]

41. Wang, Q.; Shi, W.; Zhu, B.; Su, D.S. An effective and green H$_2$O$_2$/H$_2$O/O$_3$ oxidation method for carbon nanotube to reinforce epoxy resin. *J. Mater. Sci. Technol.* **2020**, *40*, 24–30. [CrossRef]

42. Silvestro, L.; Jean Paul Gleize, P. Effect of carbon nanotubes on compressive, flexural and tensile strengths of Portland cement-based materials: A systematic literature review. *Constr. Build. Mater.* **2020**, *264*, 120237. [CrossRef]

43. Scheibe, B.; Borowiak-Palen, E.; Kalenczuk, R.J. Effect of the Silanization Processes on the Properties of Oxidized Multiwalled Carbon Nanotubes. *Acta Phys. Pol. A* **2009**, *116*, 150–155. [CrossRef]

44. Wang, Y.-L.; Stanzione, M.; Xia, H.; Buonocore, G.G.; Fortunati, E.; Kaciulis, S.; Lavorgna, M. Effect of mercapto-silanes on the functional properties of highly amorphous vinyl alcohol composites with reduced graphene oxide and cellulose nanocrystals. *Compos. Sci. Technol.* **2020**, *200*, 108458. [CrossRef]

45. Punetha, V.D.; Rana, S.; Yoo, H.J.; Chaurasia, A.; McLeskey, J.T.; Ramasamy, M.S.; Sahoo, N.G.; Cho, J.W. Functionalization of carbon nanomaterials for advanced polymer nanocomposites: A comparison study between CNT and graphene. *Prog. Polym. Sci.* **2017**, *67*, 1–47. [CrossRef]

46. Wang, Q.; Su, D.S. Reinforcing epoxy resin with activated carbon: A way of high rate of quality and price. *Compos. Commun.* **2018**, *9*, 54–57. [CrossRef]

47. Abdollahi, A.; Roghani-Mamaqani, H.; Salami-Kalajahi, M.; Mousavi, A.; Razavi, B.; Shahi, S. Preparation of organic-inorganic hybrid nanocomposites from chemically modified epoxy and novolac resins and silica-attached carbon nanotubes by sol-gel process: Investigation of thermal degradation and stability. *Prog. Org. Coat.* **2018**, *117*, 154–165. [CrossRef]

48. Shabanian, M.; Kang, N.-J.; Wang, D.-Y.; Wagenknecht, U.; Heinrich, G. Synthesis, characterization and properties of novel aliphatic–aromatic polyamide/functional carbon nanotube nanocomposites via in situ polymerization. *RSC Adv.* **2013**, *3*, 20738–20745. [CrossRef]

49. Georgakilas, V.; Tiwari, J.N.; Kemp, K.C.; Perman, J.A.; Bourlinos, A.B.; Kim, K.S.; Zboril, R. Noncovalent Functionalization of Graphene and Graphene Oxide for Energy Materials, Biosensing, Catalytic, and Biomedical Applications. *Chem. Rev.* **2016**, *116*, 5464–5519. [CrossRef]

50. Zhao, J.; Wang, H.; Gao, B.; Wang, X.; Cai, Q.; Wang, X. Chemical functionalization of graphene via aryne cycloaddition: A theoretical study. *J. Mol. Model.* **2012**, *18*, 2861–2868. [CrossRef]

51. Sainsbury, T.; Passarelli, M.; Naftaly, M.; Gnaniah, S.; Spencer, S.J.; Pollard, A.J. Covalent Carbene Functionalization of Graphene: Toward Chemical Band-Gap Manipulation. *ACS Appl. Mater. Interfaces* **2016**, *8*, 4870–4877. [CrossRef]

52. Borisov, A.S.; Hazendonk, P.; Hayes, P.G. Solid-State Nuclear Magnetic Resonance Spectroscopy: A Review of Modern Techniques and Applications for Inorganic Polymers. *J. Inorg. Organomet. Polym. Mater.* **2010**, *20*, 183–212. [CrossRef]

53. Gladysz, G.M.; Chawla, K.K. 8-Void characterization techniques. In *Voids in Materials*, 2nd ed.; Gladysz, G.M., Chawla, K.K., Eds.; Elsevier: Amsterdam, The Netherlands, 2021; pp. 167–187. [CrossRef]

54. Adams, F.; Barbante, C. Chapter 3-History and Present Status of Micro- and Nano-Imaging Analysis. In *Comprehensive Analytical Chemistry*; Adams, F., Barbante, C., Eds.; Elsevier: Amsterdam, The Netherlands, 2015; pp. 67–124. [CrossRef]

55. Sinha, P.; Datar, A.; Jeong, C.; Deng, X.; Chung, Y.G.; Lin, L.-C. Surface Area Determination of Porous Materials Using the Brunauer–Emmett–Teller (BET) Method: Limitations and Improvements. *J. Phys. Chem. C* **2019**, *123*, 20195–20209. [CrossRef]

56. Li, Z.-X.; Zhang, X.; Liu, Y.-C.; Zou, K.-Y.; Yue, M.-L. Controlling the BET Surface Area of Porous Carbon by Using the Cd/C Ratio of a Cd–MOF Precursor and Enhancing the Capacitance by Activation with KOH. *Chem.–Eur. J.* **2016**, *22*, 17734–17747. [CrossRef]

57. Furmaniak, S.; Gauden, P.A.; Kowalczyk, P.; Patrykiejew, A. Monte Carlo study of chemical reaction equilibria in pores of activated carbons. *RSC Adv.* **2017**, *7*, 53667–53679. [CrossRef]

58. Ma, P.C.; Kim, J.-K.; Tang, B.Z. Functionalization of carbon nanotubes using a silane coupling agent. *Carbon* **2006**, *44*, 3232–3238. [CrossRef]

59. Ambrosi, A.; Chua, C.K.; Bonanni, A.; Pumera, M. Lithium Aluminum Hydride as Reducing Agent for Chemically Reduced Graphene Oxides. *Chem. Mater.* **2012**, *24*, 2292–2298. [CrossRef]

60. Hoepfner, J.C.; Pezzin, S.H. Functionalization of carbon nanotubes with (3-glycidyloxypropyl)-trimethoxysilane: Effect of wrapping on epoxy matrix nanocomposites. *J. Appl. Polym. Sci.* **2016**, *133*, 44245. [CrossRef]

61. Yu, Z.-Q.; You, S.-L.; Baier, H. Effect of organosilane coupling agents on microstructure and properties of nanosilica/epoxy composites. *Polym. Compos.* **2012**, *33*, 1516–1524. [CrossRef]

62. Velasco-Santos, C.; Martinez-Hernandez, A.L.; Castano, V.M. Silanization of Carbon Nanotubes: Surface Modification and Polymer Nanocomposites. In *Carbon Nanotubes-Polymer Nanocomposites*; Yellampalli, S., Ed.; InTech: London, UK, 2011. [CrossRef]

63. Nayak, L.; Rahaman, M.; Giri, R. Surface Modification/Functionalization of Carbon Materials by Different Techniques: An Overview. In *Carbon-Containing Polymer Composites*; Rahaman, M., Khastgir, D., Aldalbahi, A.K., Eds.; Springer: Singapore, 2019; pp. 65–98. [CrossRef]

64. Velasco-Santos, C.; Martinez-Hernandez, A.L.; Brostow, W.; Castaño, V.M. Influence of Silanization Treatment on Thermomechanical Properties of Multiwalled Carbon Nanotubes: Poly(methylmethacrylate) Nanocomposites. *J. Nanomater.* **2011**, *2011*, e928659. [CrossRef]

65. Ganguly, A.; Sharma, S.; Papakonstantinou, P.; Hamilton, J. Probing the Thermal Deoxygenation of Graphene Oxide Using High-Resolution In Situ X-ray-Based Spectroscopies. *J. Phys. Chem. C* **2011**, *115*, 17009–17019. [CrossRef]

66. Spectroscopic Tools. Available online: https://www.science-and-fun.de/tools/ (accessed on 30 October 2023).

67. CHUNLIWANG991, FTIR Functional Group Database Table with Search-InstaNANO. 2021. Available online: https://instanano.com/all/characterization/ftir/ftir-functional-group-search/ (accessed on 30 October 2023).

68. Silverstein, R.M.; Bassler, G.C. Spectrometric identification of organic compounds. *J. Chem. Educ.* **1962**, *39*, 546. [CrossRef]

69. Smith, B.C. *Infrared Spectral Interpretation: A Systematic Approach*; CRC Press: Boca Raton, FL, USA, 1998. [CrossRef]

70. Colthup, N.B.; Daly, L.H.; Wiberley, S.E. Chapter 10-Ethers, Alcohols, and Phenols. In *Introduction to Infrared and Raman Spectroscopy*, 3rd ed.; Colthup, N.B., Daly, L.H., Wiberley, S.E., Eds.; Academic Press: San Diego, CA, USA, 1990; pp. 327–337. [CrossRef]

71. Bhattacharyya, I.M.; Ron, I.; Chauhan, A.; Pikhay, E.; Greental, D.; Mizrahi, N.; Roizin, Y.; Shalev, G. A new approach towards the Debye length challenge for specific and label-free biological sensing based on field-effect transistors. *Nanoscale* **2022**, *14*, 2837–2847. [CrossRef]

72. Park, J.; Park, J.; Lee, J.; Lim, C.; Lee, D.W. Size compatibility and concentration dependent supramolecular host–guest interactions at interfaces. *Nat. Commun.* **2022**, *13*, 112. [CrossRef]

73. Ganjoo, R.; Sharma, S.; Kumar, A.; Daouda, M.M.A. Activated Carbon: Fundamentals, Classification, and Properties. Available online: https://books.rsc.org/books/edited-volume/2104/chapter/7568125/Activated-Carbon-Fundamentals-Classification-and (accessed on 2 September 2024).

74. Atif, M.; Haider, H.; Bongiovanni, R.; Fayyaz, M.; Razzaq, T.; Gul, S. Physisorption and chemisorption trends in surface modification of carbon black. *Surf. Interfaces* **2022**, *31*, 102080. [CrossRef]

75. Perovic, M.; Qin, Q.; Oschatz, M. From Molecular Precursors to Nanoparticles—Tailoring the Adsorption Properties of Porous Carbon Materials by Controlled Chemical Functionalization. *Adv. Funct. Mater.* **2020**, *30*, 1908371. [CrossRef]

76. Pereira, C.; Silva, J.F.; Pereira, A.M.; Araújo, J.P.; Blanco, G.; Pintado, J.M.; Freire, C. [VO(acac)2] hybrid catalyst: From complex immobilization onto silica nanoparticles to catalytic application in the epoxidation of geraniol. *Catal. Sci. Technol.* **2011**, *1*, 784–793. [CrossRef]

77. Chen, X.; Wang, X.; Fang, D. A review on C1s XPS-spectra for some kinds of carbon materials. *Fuller. Nanotub. Carbon Nanostruct.* **2020**, *28*, 1048–1058. [CrossRef]

78. Gaspar, H.; Pereira, C.; Rebelo, S.L.H.; Pereira, M.F.R.; Figueiredo, J.L.; Freire, C. Understanding the silylation reaction of multi-walled carbon nanotubes. *Carbon* **2011**, *49*, 3441–3453. [CrossRef]

79. Gengenbach, T.R.; Major, G.H.; Linford, M.R.; Easton, C.D. Practical guides for x-ray photoelectron spectroscopy (XPS): Interpreting the carbon 1s spectrum. *J. Vac. Sci. Technol. A* **2021**, *39*, 013204. [CrossRef]

80. Howarter, J.A.; Youngblood, J.P. Optimization of Silica Silanization by 3-Aminopropyltriethoxysilane. *Langmuir* **2006**, *22*, 11142–11147. [CrossRef]

81. Durand, N.; Mariot, D.; Améduri, B.; Boutevin, B.; Ganachaud, F. Tailored Covalent Grafting of Hexafluoropropylene Oxide Oligomers onto Silica Nanoparticles: Toward Thermally Stable, Hydrophobic, and Oleophobic Nanocomposites. *Langmuir* **2011**, *27*, 4057–4067. [CrossRef]

82. Rahman, I.A.; Vejayakumaran, P.; Sipaut, C.S.; Ismail, J.; Chee, C.K. Effect of the drying techniques on the morphology of silica nanoparticles synthesized via sol–gel process. *Ceram. Int.* **2008**, *34*, 2059–2066. [CrossRef]

83. Singh, M.; Kaur, N.; Comini, E. The role of self-assembled monolayers in electronic devices. *J. Mater. Chem. C* **2020**, *8*, 3938–3955. [CrossRef]

84. Liu, Y. Self-assembled Monolayers. In *Encyclopedia of Tribology*; Wang, Q.J., Chung, Y.-W., Eds.; Springer: Boston, MA, USA, 2013; pp. 2997–3001. [CrossRef]

85. Araújo, T.; Parnell, A.J.; Bernardo, G.; Mendes, A. Cellulose-based carbon membranes for gas separations-Unraveling structural parameters and surface chemistry for superior separation performance. *Carbon* **2023**, *204*, 398–410. [CrossRef]

86. Kovtun, A.; Jones, D.; Dell'Elce, S.; Treossi, E.; Liscio, A.; Palermo, V. Accurate chemical analysis of oxygenated graphene-based materials using X-ray photoelectron spectroscopy. *Carbon* **2019**, *143*, 268–275. [CrossRef]